

COMPARISON OF EXPERIMENTAL LOSSES AMONG SIX DIFFERENT TOPOLOGIES FOR A 1.6kW BOOST CONVERTER, USING IGBT'S

Carlos A. Canesin (✱), and Ivo Barbi (✧)

(✧) Federal University of Santa Catarina
 UFSC-INEP - P.O. Box 5119 -FAX:(55) 48-2319770
 E-mail: ivo@lamep.ufsc.br
 88040-970 - Florianópolis (SC) BRAZIL

ABSTRACT

This paper presents a comparative analysis of experimental losses between a new ZCS-PWM boost converter and five different boost topologies, using IGBT's, rated at 1.6kW and operating at 20kHz.

The advantages of the new ZCS-PWM technique employing IGBT's are presented. This new ZCS operation can reduce the average total power dissipation in the devices, practically by half, when compared with the Hard-switching method.

This new ZCS-PWM boost converter is suitable for high power applications using IGBT's in power factor correction.

The principle of operation, experimental results, and comparative analysis of the new ZCS-PWM boost converter are also provided.

1. INTRODUCTION

Soft-commutation techniques have been of great interest within the last few years in switching power supply applications. However, circulating reactive energy causes large conduction losses[1].

For high power applications (above 1kW) IGBT's are preferred when compared with power MOSFET's, which present much higher conduction losses than IGBT's. On the other hand, IGBT's are relatively slow in switching speed, so the switching losses and the high frequency of operation are two well known drawbacks[2]. Therefore, to be able to operate at high frequency, soft-commutation techniques are investigated for IGBT's in resonant converter topologies.

The Zero-Voltage Switching (ZVS) technique is presented in [3,4] and the performance of the ZVT-PFC using IGBT's is analyzed in [4].

A simple scheme based on the use of fast MOSFET's to obtain a Soft-switching of IGBT's is presented in [5]. The efficiency obtained depends on the dynamic characteristics, delay time used, and drain-source on resistance ($R_{ds(on)}$) of the employed MOSFET's.

A comparative study of switching losses of IGBT's under Soft-switching (ZVS and ZCS) and Hard-switching is presented in [6]. Those results verify that the turn-off losses in Zero-current switching (ZCS) were significantly reduced, but the turn-on losses were practically the same as those for the Hard-switching technique.

A new principle was introduced in [7] to achieve Zero-current switching at constant frequency using IGBT's for high power applications. In that paper an analysis, example design, and experimental results of the new ZCS-PWM boost converter were presented with practically zero turn-on and turn-off losses.

This paper presents a comparative analysis of experimental switching losses between the new ZCS-PWM boost converter [7] and five different boost topologies, using IGBT's, rated at 1600W and operating at 20kHz.

2. THE NEW ZCS-PWM BOOST CONVERTER

Figure 1 shows the new ZCS-PWM Boost converter [7]. It is formed by two bi-directional switches S1 and S2, two diodes D1 and D2, two resonant inductors Lr1 and Lr2, and one resonant capacitor Cr. S1 is the main switch, which is responsible for the power transferred to the load, while S2 is an auxiliary switch, rated at a small average current.

One can notice that the Frequency-Modulated Quasi-Resonant-ZCS boost converter (FM-ZCS-QRC) can be derived from the new ZCS-PWM converter, and that the conventional Hard-Switching-PWM boost converter can be derived from the FM-ZCS-QRC. Therefore the new ZCS-PWM converter is a more general topology, and it incorporates the most desirable properties of the previous circuits, namely low conduction losses and PWM from the conventional one and soft-commutation from the ZCS-QRC[7].

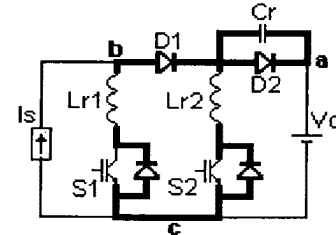


Fig.1 - New ZCS-PWM Boost converter.

Two parameters α and β are defined as follows [7]:

$$\alpha = \frac{I_s}{V_o} \sqrt{\frac{L_{r2}}{C_r}} \quad (1)$$

$$\beta = \frac{L_{r2}}{L_{r1}} \quad (2)$$

The nine topological stages are shown in Figure 2, where the main switch S1 starts conducting at $t = t_0$ and the auxiliary switch S2 at $t = t_2$. Both switches turn off simultaneously during the time interval $\Delta t_6 = t_6 - t_5$. We can notice that the complete description of these stages are in [7].

From [7], the following constraints should be satisfied to achieve soft-commutation at zero-current for both active switches, of the described operation mode.

$$\beta < 1 \quad (03)$$

and,
$$\alpha < \beta \quad (04)$$

(✱)Paulista State University - UNESP, and Ph.D. student at UFSC-INEP
 FEIS-DEE - 15378 - Ilha Solteira(SP) - BRAZIL - FAX: (55) 187-622125

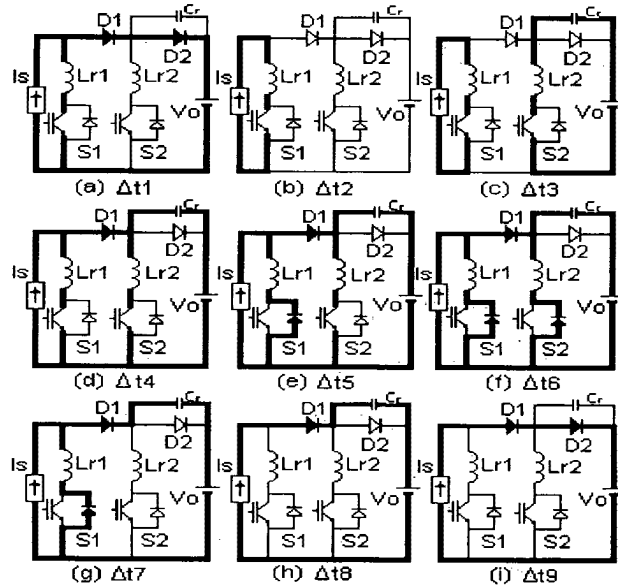


Fig.2 - The topological stages of the new ZCS-PWM boost converter.

The ideal relevant waveforms of the new ZCS-PWM boost converter are shown in Figure 3.

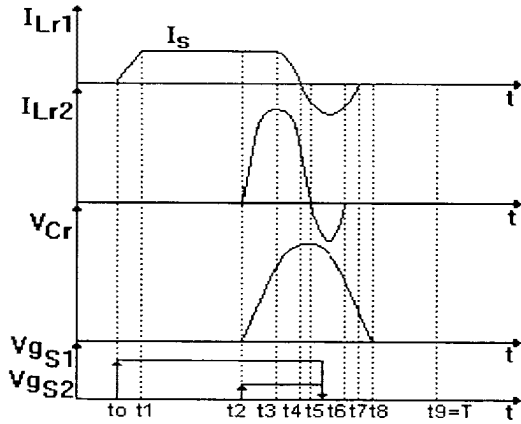


Fig.3 - Ideal relevant waveforms.

By analysis we obtain the DC voltage-conversion-ratio [7], given by equation (05).

$$q = \frac{V_o}{V_m} = \frac{1}{(1-D) - \frac{1}{2\pi} \frac{f_s}{f_{01}} \left\{ A - B + \frac{\omega_{03} \Delta t_7}{\sqrt{\beta}} \right\}} \quad (05)$$

where:
$$A = \frac{\alpha}{2\beta} + \frac{1}{\alpha} + \frac{\pi}{2} + \frac{[2\pi - a \cos(-\beta)]}{\sqrt{\beta+1}}$$

$$B = \frac{1}{\alpha} \left[\sqrt{\beta} \sin \omega_{03} \Delta t_7 + \sqrt{1-\beta} \cos \omega_{03} \Delta t_7 \right]$$

and,
$$f_{01} = \frac{\omega_{01}}{2\pi} \quad (06)$$

$$\omega_{01} = \frac{1}{\sqrt{L_{r2} C_r}} \quad (07)$$

$$\omega_{03} \Delta t_7 = a \sin \left[\sqrt{\beta - \alpha^2} - \alpha \sqrt{\frac{1-\beta}{\beta}} \right] \quad (08)$$

$$D = \frac{\Delta t_2}{T} \quad (09)$$

where: D= duty-cycle; T= switching period; f_s = switching frequency.

3. OTHER SOFT-SWITCHING AND HARD-SWITCHING BOOST TOPOLOGIES

In order to provide a comparative analysis, five different boost topologies, shown in Figure 4, were designed with the same frequency, input and output data, and operating at the same main switch. Different control methods were employed for the various topologies. The gate drive circuits for the main switch were the same.

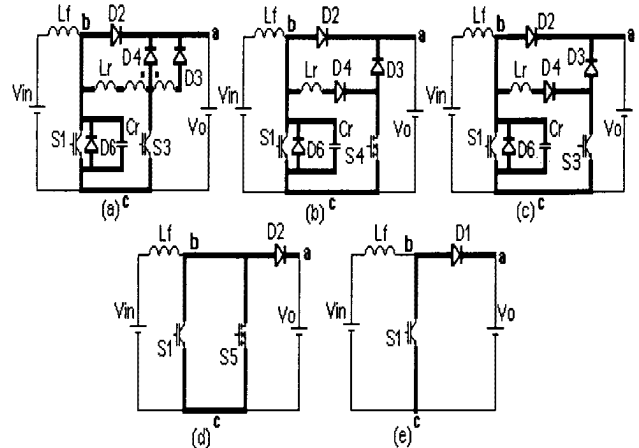


Fig.4 - (a)The ZVS-PWM; (b)The ZVT-PWM; (c)The ZVT-PWM (using two IGBT's); (d)The Soft-switching PWM (using a fast MOSFET), and (e)The conventional Hard-Switching PWM, boost converters.

In the ZVS-PWM boost converter, shown in Figure 4.a, the auxiliary cell proposed by [3] incorporates the advantages of offering soft-commutation for the main switch (ZVS) and auxiliary switch (ZCS). The current through auxiliary switch (S3) becomes zero naturally, and the main switch (S1) is gated as a dual-thyristor.

The ZVT-PWM boost converter proposed by [4], shown in Figure 4.b, allows soft-commutation (ZVS) for the main switch (S1). However, in this circuit the auxiliary switch (S4) does not benefit from the soft-commutation. The control technique demands an independent gate circuit for the auxiliary switch.

Figure 4.c shows a ZVT-PWM boost converter based on [4], where the auxiliary MOSFET was replaced with an IGBT. The auxiliary switch in this converter turns on at zero-current switching, however it's turn-off is hard-switching. Therefore, using an IGBT at S3, it's efficiency becomes smaller than that obtained in the circuit shown in Figure 4.b.

The technique analyzed in [5] and shown in Figure 4.d is very simple and provides a soft-switching of the IGBT switch (S1) through the use of a fast MOSFET switch (S5). Therefore, the efficiency of this scheme depends on the intrinsic characteristics of the employed MOSFET, and of the delay time applied at its gate circuit.

Figure 4.e shows a conventional Hard-Switching boost converter employing IGBT's. Due to the characteristics of IGBT's, the most important being its slow switching speed and tail current, the efficiency in this conventional topology is very low.

4. SPECIFICATIONS AND PARAMETERS OF THE IMPLEMENTED CIRCUITS

The input and output data specifications for all implemented converters are as follows:

$$V_{in} = 220V (\text{input voltage}); \quad V_o = 400V (\text{output voltage});$$

$$P_{out} = 1600W (\text{nominal output power}); \quad f_s = 20kHz.$$

With this data the converters analyzed were implemented using the same main switch (APT40GF100) and gate drive circuit.

The specified components and the values of the parameters for the implemented circuits are summarized in Table I. In all implemented converters the boost input inductors and the output filters were maintained with the same values.

5. EXPERIMENTAL METHODOLOGY AND RESULTS

The method used for measurement of the experimental switching energy losses was similar to that employed in [6]. The instrumentation used was the AM503-Tektronix current probe amplifier and Tektronix 2430A oscilloscope. Firstly, the oscilloscope multiplies the current through and voltage across the analyzed switch and then integrates that product. This value is equal to the energy in the component from the set time interval.

Figure 5 shows the main experimental waveforms from the new implemented ZCS-PWM boost converter, shown in Figure 1. Figures 5.a and 5.b show the turn-on and turn-off instants respectively, at the main switch (S1). Figures 5.c and 5.d show the turn-on and turn-off instants respectively, at the auxiliary switch (S2).

The experimental results, shown in Figure 5, demonstrate that the zero-current switching is achieved at constant frequency for both active switches (S1 and S2).

Figure 6 shows the relevant experimental waveforms from the implemented ZVS-PWM boost converter, shown in Figure 4.a. Figures 6.a and 6.b show the turn-on and turn-off instants respectively, at the main switch (S1). Figure 6.c shows the turn-on and turn-off instants at the auxiliary switch (S3). Figure 6.d shows the current through and voltage across the passive switch (diode D2).

From experimental results shown in Figure 6, one can demonstrate that the zero-voltage switching is achieved for the main switch (S1) and the passive switch (D2), and zero-current switching is achieved for the auxiliary switch (S3).

Figure 7 shows the main experimental waveforms from the implemented ZVT-PWM boost converter, shown in Figure 4.b. Figures 7.a and 7.b show the turn-on and turn-off details respectively, at the main switch (S1). Figure 7.c shows the turn-on and turn-off instants, while Figure 7.d shows only the turn-off detail at the auxiliary switch (S4).

The experimental results shown in Figure 7, demonstrate that zero-voltage switching is achieved for the main switch (S1). The turn-on at the auxiliary switch (S4) is a zero-current switching, however the turn-off, shown in Figure 7.d, verified that the auxiliary switch (S4) does not benefit from the soft-commutation.

TABLE I
COMPONENTS AND PARAMETERS FOR THE IMPLEMENTED BOOST CONVERTERS

		New ZCS-PWM Figure 1	ZVS-PWM Figure 4.a	ZVT-PWM Figure 4.b	ZVT-PWM (two IGBT's) Figure 4.c	IGBT+MOSFET Figure 4.d	Hard-switching Figure 4.e
S1	main switch	APT40GF100	APT40GF100	APT40GF100	APT40GF100	APT40GF100	APT40GF100
S2	auxiliary switch	IGTP10N50A	—	—	—	—	—
S3	auxiliary switch	—	HGTG24N80	—	HGTG24N80	—	—
S4	auxiliary switch	—	—	IRF460	—	—	—
S5	auxiliary switch	—	—	—	—	BUZ355	—
D1	diode	MUR 850	—	—	—	—	MUR 850
D2	diode	APT15D100	APT15D100	APT15D100	APT15D100	APT15D100	—
D3	diode	—	MUR8100	MUR8100	MUR8100	—	—
D4	diode	—	MUR8100	MUR8100	MUR8100	—	—
D5	diode	MUR150	—	—	—	—	—
D6	diode	—	APT15D100	APT15D100	APT15D100	—	—
Lr	resonant inductor	—	60uH(E30/14)	60uH(E30/14)	60uH(E30/14)	—	—
Lr1	resonant inductor	71 6uH(E30/14)	—	—	—	—	—
Lr2	resonant inductor	49uH(E30/7)	—	—	—	—	—
Cr	resonant capacitor	59nF(1.8kV)	22nF(E30V)	22nF(E30V)	22nF(E30V)	—	—
Tr	auto transformer	—	E42/15 Np=30 turns Ns=91 turns	—	—	—	—
Lf	input filter	1.75mH(E65/39)	1.75mH(E65/39)	1.75mH(E65/39)	1.75mH(E65/39)	1.75mH(E65/39)	1.75mH(E65/39)
Cf	output filter	470uF(500V)	470uF(500V)	470uF(500V)	470uF(500V)	470uF(500V)	470uF(500V)

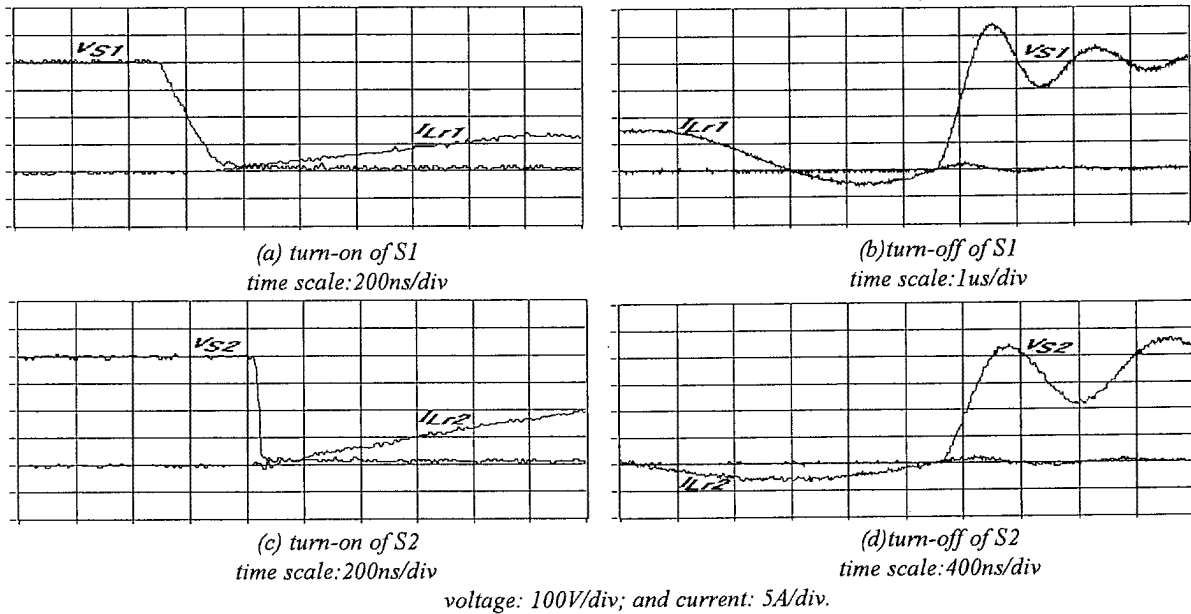


Fig.5 -Experimental waveforms for the New ZCS-PWM boost converter(Fig.1).

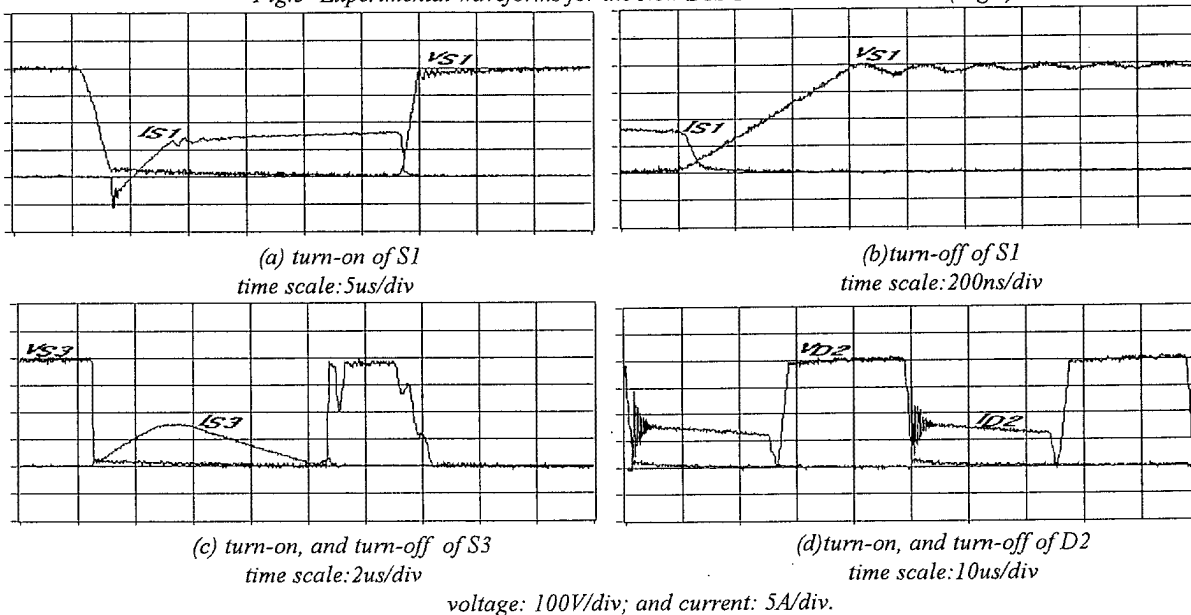


Fig.6 -Experimental waveforms for the ZVS-PWM boost converter(Fig.4.a).

Figure 8 shows the relevant experimental waveforms from the implemented ZVT-PWM boost converter which employs IGBTs for both main and auxiliary switches, shown in Figure 4.c.

Figures 8.a and 8.b show the turn-on and turn-off instants respectively, at the main switch (S1).

One can verify in the Figures 8.a and 8.b that the zero-voltage switching is achieved for the main switch (S1).

The auxiliary switch (S3) commutes softly (ZCS) during its turn-on, as one can see in Figure 8.c. However its turn-off due to the presence of the tail current, shown in Figure 8.d, reduces the efficiency in this topology.

Figures 9.a and 9.b show the turn-on and turn-off details respectively, at the main switch (S1). Figures 9.c and 9.d show the turn-on and turn-off instants respectively, at the auxiliary switch

(S5), for the implemented boost converter using a fast auxiliary MOSFET (S5) to obtain a soft-switching of the main switch (S1), shown in Figure 4.d.

The experimental results shown in Figure 9.a demonstrate that the turn-on losses were reduced, and Figure 9.b verifies that the turn-off losses were practically zero, at the main switch (S1).

The experimental results shown in Figures 9.c and 9.d demonstrate that the turn-on and turn-off losses respectively, at the auxiliary switch (S5) are not negligible. One can notice that through a better selection for the auxiliary MOSFET (S5) it is possible to obtain an improvement in this topology.

Figure 10 shows the turn-on and turn-off details of the switch (S1) for the conventional Hard-Switching boost converter, shown in Figure 4.e.

The experimental results of the turn-on and turn-off energy losses are summarized in Table II for all devices of the new ZCS-PWM and remaining implemented boost converters.

The average power dissipation for IGBT's (P_{av1}) is given by equation (10), for MOSFET's (P_{av2}) is given by equation (11), and for Ultra-Fast Diode (P_{av3}) is given by equation (12).

$$P_{av1} = I_{c_{av}} V_{ce_{on}} + f_s (W_{on} + W_{off}) \quad (10)$$

$$P_{av2} = I_{d_{rms}}^2 R_{ds_{on}} + f_s (W_{on} + W_{off}) \quad (11)$$

where:

$I_{c_{av}}$ = average collector current;

$I_{d_{rms}}$ = rms drain current;

$V_{ce_{on}}$ = collector-to-emitter saturation voltage;

$R_{ds_{on}}$ = drain-source on-resistance;

W_{on} = turn-on switching losses;

W_{off} = turn-off switching losses.

$$P_{av3} = I_F V_F + f_s (W_{d_{on}} + W_{d_{off}}) \quad (12)$$

where:

I_F = average forward current;

V_F = forward voltage.

It should be pointed out that the equations above have a simplified formula for the power conduction losses in the devices, however these simplifications were maintained for all comparative analysis.

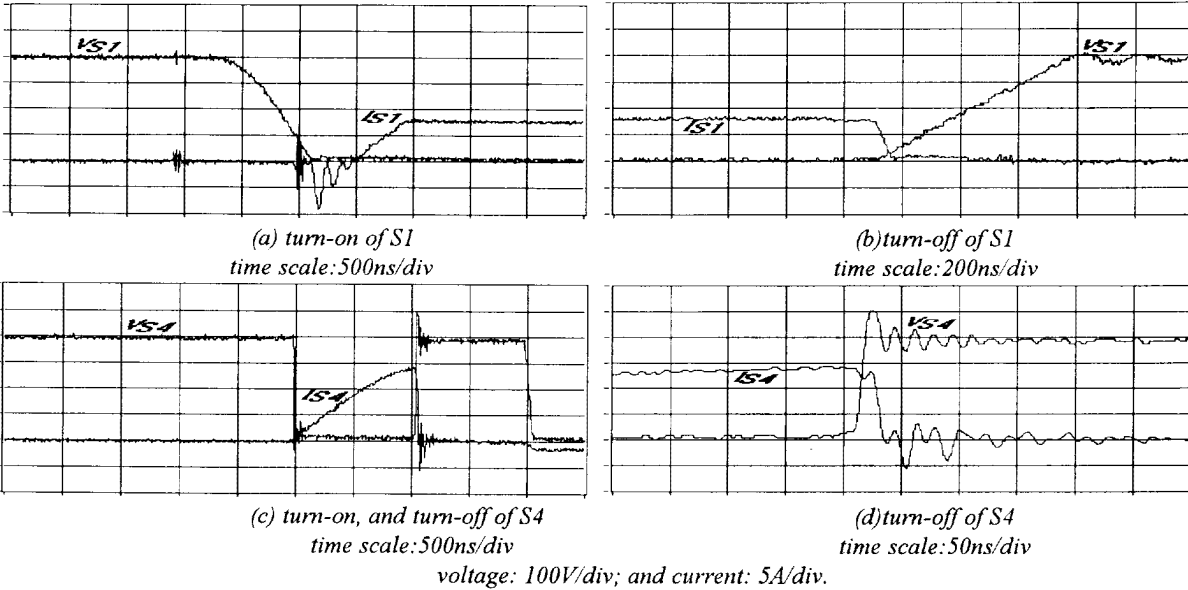


Fig.7 -Experimental waveforms for the ZVT-PWM boost converter(Fig.4.b).

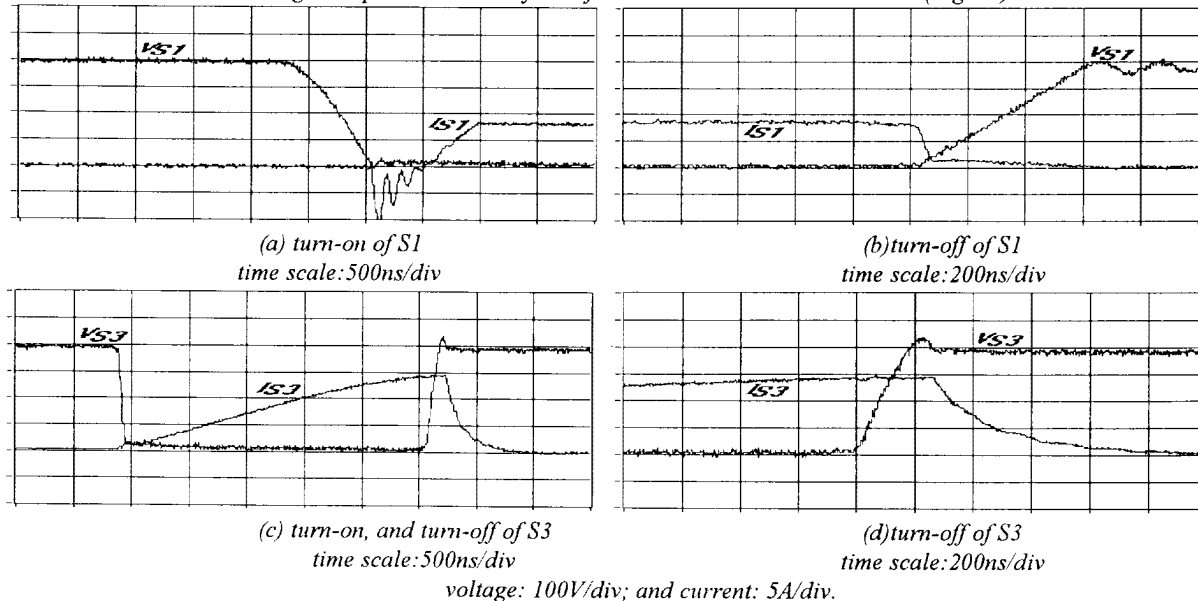


Fig.8 -Experimental waveforms for the ZVT-PWM boost converter, using two IGBT's(Fig.4.c).

6. ANALYSIS OF EXPERIMENTAL RESULTS

With the experimental results of the turn-on and turn-off switching energy losses summarized in Table II, one can obtain the average total power dissipation in the devices (P_{avT}), as function of the switching frequency, shown in Figure 11, for all implemented topologies analyzed.

The results shown in Figure 11 demonstrate that only the ZVS-PWM technique proposed in [3] has a similar result in comparison with the new ZCS-PWM boost converter proposed in [7]. However, for this set output power, and for switching frequency greater than 25kHz, the benefits of the new ZCS-PWM technique can be verified.

This new ZCS-PWM boost converter provides a better efficiency in relation to all other implemented topologies, and it is suitable for high power applications, operating with high switching frequency values.

Therefore, in a general comparison, for switching frequency greater than 6kHz the advantages of this new ZCS-PWM boost converter [7] can be clearly verified in Figure 11.

7. CONCLUSION

This paper has presented a comparative analysis of experimental losses between a new ZCS-PWM boost converter and five other different boost topologies, using IGBT's.

Theoretical studies and comparative experimental results for this new ZCS-PWM boost converter, allow us to draw the following conclusions:

- Soft-commutation (ZCS) is achieved for the active switches, from non-load up to full load;
- Latching of IGBT's due to turn-off never occurs, this relieves the RBSOA stress of that one;
- The converter is regulated by the conventional PWM technique, at constant frequency;
- Low conduction losses are verified;
- The passive switches also commuted softly (ZVS);

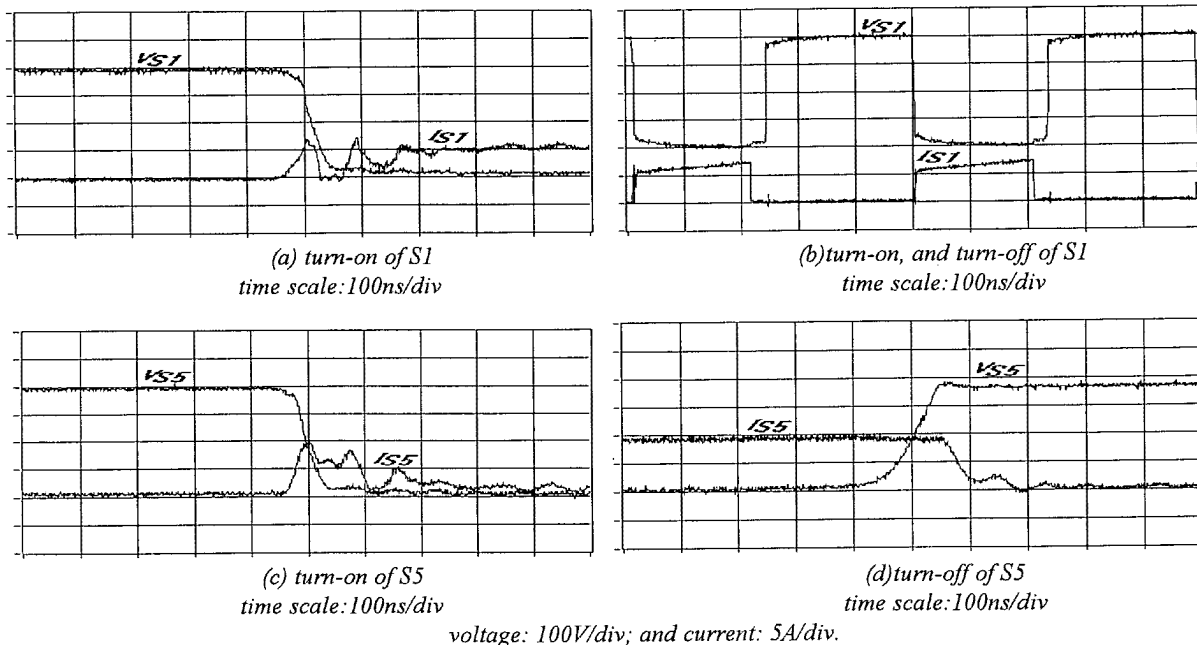


Fig.9 -Experimental waveforms for the boost converter with the help of MOSFET (Fig.4.d).

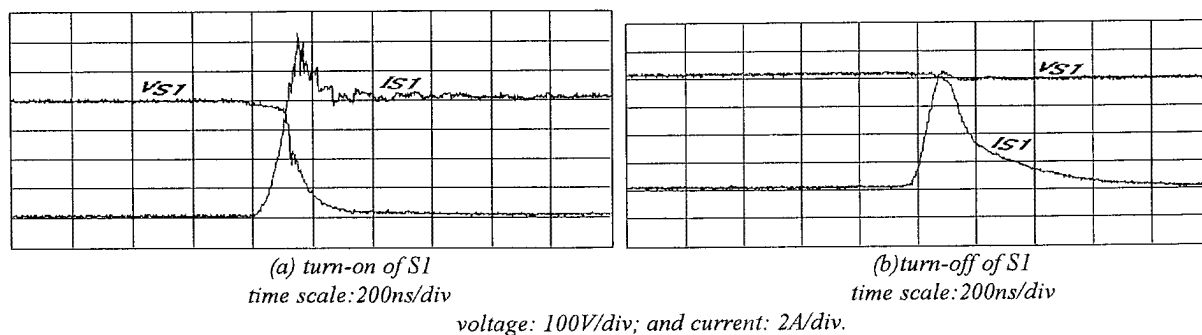


Fig.10 -Experimental waveforms for the Hard-switching boost converter (Fig.4.e).

TABLE II
SWITCHING ENERGY LOSSES (*)

CONVERTER	DEVICE	(a) Figure 1		(b) Figure 4.a		(c) Figure 4.b		(d) Figure 4.c		(e) Figure 4.d		(f) Figure 4.e	
		On (mJ)	Off (mJ)	On (mJ)	Off (mJ)	On (mJ)	Off (mJ)	On (mJ)	Off (mJ)	On (mJ)	Off (mJ)	On (mJ)	Off (mJ)
S1	AP340GF100	~0	0	0	3e-2	0	2.5e-2	0	2.5e-2	3e-2	0	39e-2	81.6e-2
D1	MUR 850	0	0	—	—	—	—	—	—	—	—	~0	10e-2
S2	IGTP10N50A	~0	0	—	—	—	—	—	—	—	—	—	—
D2	APT15D100	0	0	0	0	0	0	0	0	~0	~0	—	—
S3	HGTG24N80	—	—	0	0	—	—	0	110e-2	—	—	—	—
S4	IRF480	—	—	—	—	0	36e-2	—	—	—	—	—	—
S5	BUZ355	—	—	—	—	—	—	—	—	16.5e-2	65e-2	—	—
D3	MUR8100	—	—	0	0	0	0	0	0	—	—	—	—
D4	MUR8100	—	—	0	0	0	0	0	0	—	—	—	—

* Tektronix2430A oscilloscope, and AM503 Current probe amplifier.

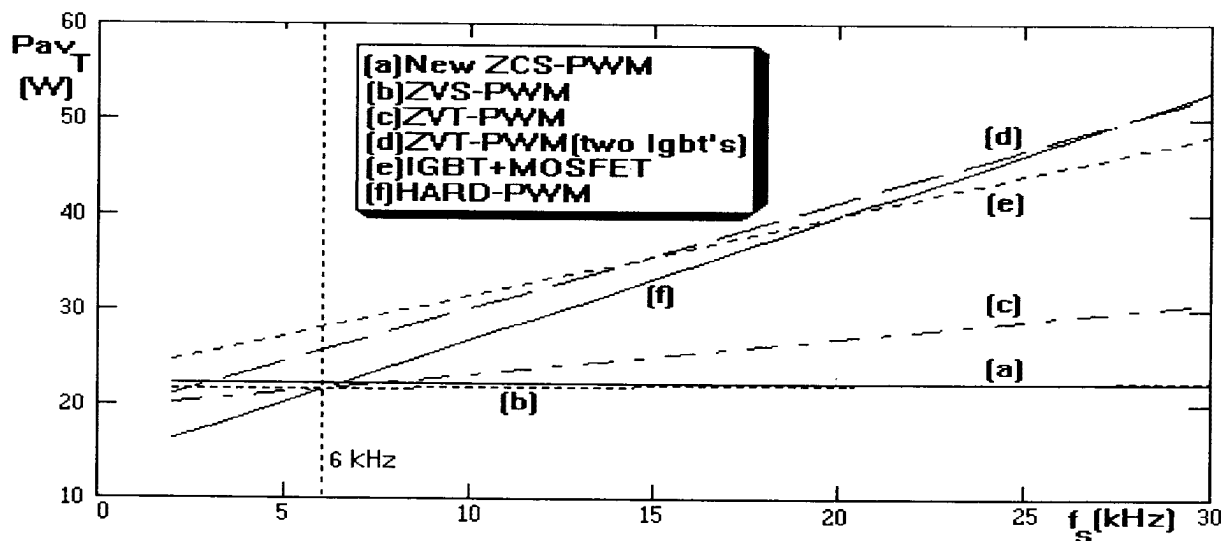


Fig.11 -Average total power dissipation in the devices.

■ Average total power dissipation in the devices can be reduced by more than half, when compared with Hard-Switching. Thus, providing a great reduction in the heatsinks;

■ In general, it presented less average total power dissipation in the devices for f_s greater than 6kHz, in comparison with the tested techniques.

So, the new ZCS-PWM boost converter combines the advantages of the PWM and ZCS techniques, without additional current and voltage stresses, in comparison with the conventional hard-switching converter, and maintaining high efficiency.

The new ZCS-PWM boost converter is appropriate for high power and power factor correction applications.

REFERENCES

[1] F. C. Lee, "High-Frequency Quasi-Resonant Converter Technologies", Proceedings of the IEEE, pp. 377-390, 1988;

[2] R. Rangan, D. Y. Chen, J. Yang and J. Lee, "Application of Insulated Gate Bipolar Transistor to Zero-Current switching converters", IEEE Transactions on Power Electronics, pp. 02-07, January 1989;

[3] D. C. Martins, F. J. M. Seixas, J. A. Brilhante and I. Barbi, "A Family of DC/DC PWM converters using a new ZVS commutation cell", IEEE PESC RECORDS, pp. 524-530, 1993;

[4] G. Hua, C. S. Leu, Y. Jiang and F. C. Lee, "Novel zero-voltage-transition PWM converters", IEEE Transactions on Power Electronics, pp. 213-219, March 1994;

[5] Y. Jiang, G. Hua, E. Yang and F. C. Lee, "Soft-switching of IGBT's with the help of MOSFET's in bridge-type converters", IEEE PESC RECORDS, pp. 151-157, 1993;

[6] F. C. Lee, K. Wang, G. Hua and D. Borojovic, "A comparative study of switching losses of IGBT's under Hard-switching, Zero-voltage switching and Zero-current switching", IEEE PESC RECORDS, pp. 1196-1204, 1994;

[7] C. A. Canesin, C. M. C. Duarte and I. Barbi, "A new family of pulse-width-modulated zero-current switching DC/DC converters", IEEE IPEC RECORDS, pp. 1379-1384, 1995.